Analysis of Multilayer Spherical Head Model Exposed to EM Radiation from Arbitrary Source Using Spherical Vector Wave Functions

Mohammad Alian, and Narges Noori
Department of Communication Technologies, Iran Telecommunication Research Center (ITRC), End of North Kargar St., Tehran 1439955471, Iran
Corresponding author: Narges Noori (e-mail: nnoori@itrc.ac.ir)

ABSTRACT A semi-analytical method is presented for the assessment of the induced electromagnetic field inside a multilayer spherical head model exposed to radiation of an arbitrary source antenna. First, the isolated source antenna is simulated in a full-wave software to evaluate its radiation characteristics. By sampling the radiated fields, their spherical vector wave function (SVWF) amplitudes are evaluated. Next, the well-known translation addition theorem for SVWFs is implemented to translate the SVWFs of the radiated fields to the local coordinate system of the head model. It's assumed that the presence of the head model does not affect the primary radiated fields by the antenna due to the adequate distance between them. By applying the boundary conditions on the head model, the unknown SVWF amplitudes of the induced fields inside each layer as well as those of the scattered field outside the model are evaluated. The verification of the proposed method is shown through some numerical examples. In comparison with a full-wave numerical method, the proposed method provides an efficient repeatable simulation approach due to the independent analysis of the source and head model, provided that the reaction of the head model to the antenna is negligible.

INDEX TERMS Addition theorem, Electromagnetic field exposure, Human head model, Spherical vector wave functions.

I. INTRODUCTION

THE continuous growth of demands for using wireless telecommunication devices has made them indispensable components of today's human life. The potential health hazard due to the electromagnetic radiation of such devices has always been an important issue for scientists. Particularly, electromagnetic exposure by mobile handsets in close proximity to the human head has so far been considered in many related works. Nonetheless, the health hazard due to radiation from many other devices at near distances such as radiation from personal computer equipment, wireless routers as well as mobile handsets in standby mode may also be inevitable as they usually expose the human body for a long period of time.

For a wide range of microwave frequencies, the electromagnetic waves inside biological tissues have a wavelength much smaller than the human whole body length, making many theoretical methods quite insufficient for the analysis. Accordingly, the common methods for the theoretical investigation of the electromagnetic fields inside the human body consider only a specific part of the body under electromagnetic radiation in the absence of the other parts. However, this approach ignores the multiple interactions of electromagnetic fields among different parts, it can provide a good estimation of the exact solution. Specifically, the focus of many research papers is on the effects of electromagnetic radiation on the human head due to the brain's sensitivity to electromagnetic radiation.

Theoretical methods for investigation of the human head under electromagnetic field exposure may be categorized into two types of analytical and numerical methods. Obviously, the analytical methods are only applicable to a finite number of canonical problems involving simple models of the human head and some basic models of the radiating source. Thereupon, they are usually applied as a tool for the verification of numerical methods. For example, references [1], [2] consider the problem of interaction of a dipole antenna and a multilayer spherical head model based on the expansion of dyadic Green's function in terms of spherical and planar wavefronts, respectively. However, due to the assumption of the close proximity of the source and head model in both works, the reaction of the head model to the antenna is taken into account, but the source structure has been limited to the wire antennas in both cases. Obviously, such

restricting assumptions can be found almost in all analytical methods. Accordingly, the implementation of numerical methods is inevitable for dealing with uncanonical problems in a realistic scenario. So far, numerous methods such as the method of moments (MoM) [3], [4], finite-difference time-domain (FDTD) [5], [6], finite element method (FEM) [7], [8] and etc. are used for the numerical investigation of the human body under electromagnetic field exposure. Whereas the numerical methods provide more realistic models in comparison with the analytical methods, they may be restricted by computer resources, particularly where the wavelength is much smaller than the problem electrical size as in the case of biological tissues at a wide range of microwave frequencies.

In this paper, a semi-analytical method is proposed for the investigation of the induced electromagnetic field inside the human head, exposed to radiation by an arbitrary source antenna. Similar to many analytical works, a multilayer spherical head model is considered, whereas the antenna may have an arbitrary structure. An adequate distance is assumed between the source antenna and the head model to ignore the reaction of the model to the antenna's primary radiated fields. First, the isolated antenna is simulated numerically to evaluate the radiated fields in the absence of the head model. This makes it possible to use a commercial software to easily evaluate the antenna radiated fields. The tangential components of these radiated fields are sampled on the surface of a sphere encompassing the antenna structure. So, thanks to the uniqueness theorem, it is possible to have the radiated field at any point of space outside this surface. It has been done by extracting the SVWF amplitudes of the antenna radiated fields. Then, the amplitudes of SVWFs corresponding to the antenna coordinate system are translated to those of the head model coordinate system (with origin on the center of the head model) using the addition theorem for translation of SVWFs. Finally, the boundary conditions are considered to evaluate the amplitudes of SVWFs inside different layers of the spherical model. The performance of the proposed method may be more evident where the problem solution should be repeated with various spherical head model properties or different distances from the antenna as it can facilitate the solution without the need to repeat the antenna structure analysis. This is contrary to the full-wave numerical methods where the whole problem should be analyzed monolithically, even if the electromagnetic field interactions can be ignored.

The rest of the paper is arranged as follows. The problem analysis is presented in section II. First, the SVWF expansions of the electromagnetic fields are represented in section II-A. Then, the amplitudes of the SVWFs for radiated fields by the antenna are extracted in section II-B. The translation addition theorem is reviewed in section II-C. Section II-D considers boundary conditions on the multilayer spherical model for extraction of the SVWF amplitudes inside different layers of the head model. Numerical examples for the verification of the proposed method are presented in section III. Finally, section IV considers the conclusions.

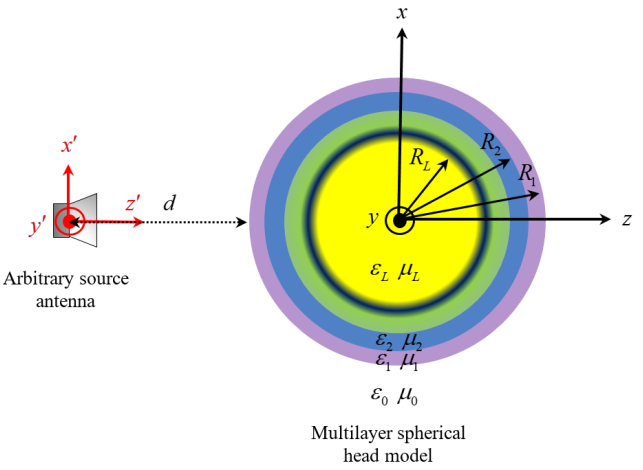

FIGURE 1. A multilayer spherical head model exposed to radiation of an arbitrary source antenna.

II. PROBLEM DESCRIPTION AND ANALYSIS

Consider Figure 1 where a multilayer spherical head model is exposed to the radiated fields by an arbitrary source antenna. The electromagnetic fields inside the spherical model are the unknowns to be evaluated. Since the proposed method considers no restriction on the source antenna, either measurement or a numerical method may be employed for the evaluation of its radiated fields. The last case which is used in this paper may be easily performed by an appropriate commercial full-wave software. Figure 2 shows the source antenna enclosed by an imaginary sampling sphere in the absence of the head model. In the first step, the electromagnetic fields radiated by this source antenna are simulated and sampled on the surface of the imaginary sphere. The amplitudes of SVWFs of the radiated fields are evaluated by weighted integrations of the radiated fields. Since these amplitudes are related to the SVWFs in the source coordinate system, the translation addition theorem of the SVWFs is applied to evaluate those of SVWFs in the coordinate system originating from the center of the spherical head model. Finally, the boundary conditions are considered on the spherical model to evaluate the amplitudes of SVWFs corresponding to the induced fields inside the head model as well as the scattered fields outside it. These steps are the subject matters of sections II-A to II-D.

A. EXPANSIONS OF ELECTRIC AND MAGNETIC FIELDS IN TERMS OF SVWFS

In an isotropic homogeneous source-free region, electric and magnetic fields may be expanded in terms of SVWFs as follows [9], [10]

$$\mathbf{E}_\ell(r,\theta,\phi) = \sum_{n=1}^{\infty}\sum_{m=-n}^{n} a_{nm,\ell}\mathbf{m}^{(i)}_{nm,\ell}(r,\theta,\phi) + b_{nm,\ell}\mathbf{n}^{(i)}_{nm,\ell}(r,\theta,\phi) \quad (1)$$

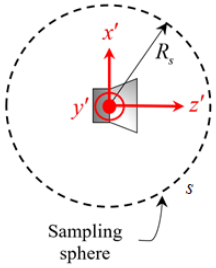

FIGURE 2. Source antenna enclosed by an imaginary sampling sphere.

$$\mathbf{H}_\ell(r,\theta,\phi) = \frac{j}{\eta_\ell}\sum_{n=1}^{\infty}\sum_{m=-n}^{n} b_{nm,\ell}\mathbf{m}_{nm,\ell}(r,\theta,\phi) + a_{nm,\ell}\mathbf{n}_{nm,\ell}(r,\theta,\phi) \tag{2}$$

where j is the imaginary unit ($j^2 = -1$), (r,θ,ϕ) show the spherical coordinates and $\eta_\ell = \sqrt{\mu_\ell/\varepsilon_\ell^c}$ with $0 \le \ell \le L$ shows the intrinsic impedance of the ℓ^{th} layer with permeability μ_ℓ and complex permittivity of $\varepsilon_\ell^c = \varepsilon_0\left(\varepsilon_{r_\ell} + \sigma_\ell/(j\omega\varepsilon_0)\right)$, where ε_0, ε_{r_ℓ}, σ_ℓ, and ω denote the permittivity of free-space, permittivity of ℓ^{th} layer, conductivity of ℓ^{th} layer, and angular frequency, respectively. Furthermore, the SVWFs, $\mathbf{m}_{nm,\ell}^{(i)}$ and $\mathbf{n}_{nm,\ell}^{(i)}$ are defined as follows [11]–[13]

$$\mathbf{m}_{mn,\ell}^{(i)} = \frac{jm}{\sin\theta} z_n^{(i)}(k_\ell r) P_n^m(\cos\theta)\exp(jm\phi)\,\hat{\boldsymbol{\theta}} - z_n^{(i)}(k_\ell r)\frac{\partial}{\partial\theta}P_n^m(\cos\theta)\exp(jm\phi)\,\hat{\boldsymbol{\phi}} \tag{3}$$

$$\mathbf{n}_{mn,\ell}^{(i)} = \frac{n(n+1)}{k_\ell r} z_n^{(i)}(k_\ell r) P_n^m(\cos\theta)\exp(jm\phi)\,\hat{\mathbf{r}} + \frac{1}{k_\ell r}\frac{\partial}{\partial r}[r z_n^{(i)}(k_\ell r)]\frac{\partial}{\partial\theta}P_n^m(\cos\theta)\exp(jm\phi)\,\hat{\boldsymbol{\theta}} + \frac{jm}{k_\ell r\sin\theta}\frac{\partial}{\partial r}[r z_n^{(i)}(k_\ell r)]P_n^m(\cos\theta)\exp(jm\phi)\,\hat{\boldsymbol{\phi}} \tag{4}$$

where $k_\ell = \omega\sqrt{\mu_\ell\varepsilon_\ell^c}$ is the wavenumber of ℓ^{th} layer, $z_n^{(i)}(\cdot)$ shows the spherical Bessel function of the first kind $j_n(\cdot)$ and spherical Hankel function of the second kind $h_n^{(2)}(\cdot)$ for $i = 1$ and $i = 4$, respectively. Furthermore, $P_n^m(\cdot)$ denotes the associated Legendre function of n^{th} degree and m^{th} order. Time dependence of $exp(j\omega t)$ is assumed throughout this paper.

B. SVWF AMPLITUDES OF THE INCIDENT FIELD

Consider Figure 2 where the source antenna is enclosed by a sampling sphere of radius R_s. The electric and magnetic fields on the surface of sampling sphere s are supposed to be known at least for their tangential components through numerical simulation of the antenna in the absence of the head model. Referring to (1) and (2), thanks to the orthogonality of SVWFs [9], the SVWF amplitudes of the incident fields may be readily evaluated from their tangential components on the surface of the sampling sphere as follows

$$a'_{\nu\mu,0} = \frac{2\nu+1}{4\pi\nu(\nu+1)}\frac{(\nu-\mu)!}{(\nu+\mu)!}\frac{1}{R_s^2|h_\nu^{(2)}(k_0R_s)|^2}\times \oint_s\left(\mathbf{m}^{*(4)}_{\nu\mu,0}\cdot\mathbf{E}_0\right)ds \tag{5}$$

$$b'_{\nu\mu,0} = \frac{2\nu+1}{4\pi\nu(\nu+1)}\frac{(\nu-\mu)!}{(\nu+\mu)!}\frac{-j\eta_0}{R_s^2|h_\nu^{(2)}(k_0R_s)|^2}\times \oint_s\left(\mathbf{m}^{*(4)}_{\nu\mu,0}\cdot\mathbf{H}_0\right)ds \tag{6}$$

where the asterisk * shows complex conjugation and $\mathbf{E}_0$ and $\mathbf{H}_0$ show the electric and magnetic fields radiated by the antenna, respectively.

It may be worth mentioning that from (1), the coefficients $b'_{\nu\mu,0}$ could also be evaluated from the tangential components of the electric field on the surface of the sampling sphere to get rid of sampling from magnetic field with a slight modification to (6).

Note that, the infinite sums on integer n in the SVWF expansions of the electric and magnetic fields in (1) and (2) can be truncated to a finite number N depending on the problem assumptions. As the proposed method ignores the reaction of the head model to the antenna due to the adequate distance between them, the truncation criterion may be considered only according to the antenna's characteristics regardless of the model properties. If r_0 is the radius of the minimum sphere enclosing the antenna, according to many previous works, such a truncation criterion may be considered as

$$N = [k_0 r_0] + N_0 \tag{7}$$

which ignores the higher order modes that their overall power is a negligible contribution of the whole power radiated by the antenna [14]–[16]. The integer number N_0 in (7) determines the required accuracy, and $[x]$ shows the first integer greater than x. The examination problems in this work reach acceptable accuracies with $N_0 = 10$.

C. TRANSLATION OF SVWFS OF THE INCIDENT FIELD

In section II-B SVWF amplitudes were evaluated in the coordinate system of the source antenna. The boundary conditions on the multilayer spherical model can be more easily analyzed in the coordinate system originating from the center of the spherical head model. So, the expansion of the fields in terms of SVWFs should also be performed in the same coordinate system. The translation addition theorem of SVWFs may be applied to translate the SVWFs from the source coordinate system to that of the head model where the origin is displaced and corresponding axes are parallel. According to this type of addition theorem, a specific SVWF

in a coordinate system may be expanded on infinite series of SVWFs in the new coordinate system as follows [17], [18]

$$\mathbf{m}^{(4)}_{\nu\mu}(r',\theta',\phi') = \sum_{n=1}^{N}\sum_{m=-n}^{n} C(\mu,\nu|m,n)\,\mathbf{m}^{(1)}_{nm,\ell}(r,\theta,\phi) + D(\mu,\nu|m,n)\,\mathbf{n}^{(1)}_{nm,\ell}(r,\theta,\phi) \tag{8}$$

$$\mathbf{n}^{(4)}_{\nu\mu}(r',\theta',\phi') = \sum_{n=1}^{N}\sum_{m=-n}^{n} D(\mu,\nu|m,n)\,\mathbf{m}^{(1)}_{nm,\ell}(r,\theta,\phi) + C(\mu,\nu|m,n)\,\mathbf{n}^{(1)}_{nm,\ell}(r,\theta,\phi) \tag{9}$$

where (r,θ,ϕ) and (r',θ',ϕ') are spherical coordinates pertaining to (x,y,z) and (x',y',z') Cartesian coordinates, respectively (refer to Figure 1). For a rigid translation, the coefficients $C(\mu,\nu|m,n)$ and $D(\mu,\nu|m,n)$ are defined in the Appendix. B. By substitution of (8) and (9) in (1) and (2), the amplitudes of SVWFs in the head model coordinate system may be evaluated in terms of those of the source antenna coordinate system as follows

$$a_{mn,0} = \sum_{\nu=1}^{N}\sum_{\mu=-\nu}^{\nu} C(\mu,\nu|m,n)\,a'_{\nu\mu,0} + D(\mu,\nu|m,n)\,b'_{\nu\mu,0} \tag{10}$$

$$b_{mn,0} = \sum_{\nu=1}^{N}\sum_{\mu=-\nu}^{\nu} D(\mu,\nu|m,n)\,a'_{\nu\mu,0} + C(\mu,\nu|m,n)\,b'_{\nu\mu,0}. \tag{11}$$

It may be worth mentioning that as the source antenna radiated fields should satisfy the propagation conditions in the far distances from the antenna, their SVWF expansions are in terms of the Hankel functions of the second kind, and superscript $i = 4$ is considered in left-hand sides of (8) and (9). However, as the antenna radiated fields should be confined at the origin of the head model coordinate system, the SVWFs for the expansion of the fields in this coordinate system should be represented in terms of the Bessel function of the first kind that is provided by superscripts $i = 1$ in the right-hand sides of (8) and (9).

D. BOUNDARY CONDITIONS

Consider the multilayer spherical head model shown in Figure 1 which is exposed to the known electromagnetic radiation of the source antenna. Since any layer is supposed to be a homogenous isotropic medium, the electric and magnetic fields may be expanded in terms of SVWFs according to (1) and (2). The boundary conditions for the electric and magnetic fields at the interface of the ℓ^{th} and $(\ell-1)^{th}$ layers in the coordinate system with origin on the center of the spherical head model are

$$\hat{\mathbf{r}}\times\left(\mathbf{E}^{inc}_{\ell}(R_\ell,\theta,\phi)+\mathbf{E}^{sca}_{\ell}(R_\ell,\theta,\phi)\right) = \hat{\mathbf{r}}\times\left(\mathbf{E}^{inc}_{\ell-1}(R_\ell,\theta,\phi)+\mathbf{E}^{sca}_{\ell-1}(R_\ell,\theta,\phi)\right) \tag{12}$$

$$\hat{\mathbf{r}}\times\left(\mathbf{H}^{inc}_{\ell}(R_\ell,\theta,\phi)+\mathbf{H}^{sca}_{\ell}(R_\ell,\theta,\phi)\right) = \hat{\mathbf{r}}\times\left(\mathbf{H}^{inc}_{\ell-1}(R_\ell,\theta,\phi)+\mathbf{H}^{sca}_{\ell-1}(R_\ell,\theta,\phi)\right) \tag{13}$$

where the superscripts inc and sca represent the incidence and scattering, respectively to distinguish the standing and outgoing waves inside each layer. Substitution of the electric fields in (12) by their expanded form of (1) results to

$$\begin{aligned}
&\sum_{n=1}^{N}\sum_{m=-n}^{n} a_{nm,\ell}\left(\hat{\mathbf{r}}\times\mathbf{m}^{(1)}_{nm,\ell}(R_\ell,\theta,\phi)\right) + b_{nm,\ell}\left(\hat{\mathbf{r}}\times\mathbf{n}^{(1)}_{nm,\ell}(R_\ell,\theta,\phi)\right) + \\
&\sum_{n=1}^{N}\sum_{m=-n}^{n} c_{nm,\ell}\left(\hat{\mathbf{r}}\times\mathbf{m}^{(4)}_{nm,\ell}(R_\ell,\theta,\phi)\right) + d_{nm,\ell}\left(\hat{\mathbf{r}}\times\mathbf{n}^{(4)}_{nm,\ell}(R_\ell,\theta,\phi)\right) = \\
&\sum_{n=1}^{N}\sum_{m=-n}^{n} a_{nm,\ell-1}\left(\hat{\mathbf{r}}\times\mathbf{m}^{(1)}_{nm,\ell-1}(R_\ell,\theta,\phi)\right) + b_{nm,\ell-1}\left(\hat{\mathbf{r}}\times\mathbf{n}^{(1)}_{nm,\ell-1}(R_\ell,\theta,\phi)\right) + \\
&\sum_{n=1}^{N}\sum_{m=-n}^{n} c_{nm,\ell-1}\left(\hat{\mathbf{r}}\times\mathbf{m}^{(4)}_{nm,\ell-1}(R_\ell,\theta,\phi)\right) + d_{nm,\ell-1}\left(\hat{\mathbf{r}}\times\mathbf{n}^{(4)}_{nm,\ell-1}(R_\ell,\theta,\phi)\right)
\end{aligned} \tag{14}$$

where for the ℓ^{th} layer, the amplitudes of SVWFs of the standing wave are shown by $a_{nm,\ell}$ and $b_{nm,\ell}$, and those of outgoing waves are shown by $c_{nm,\ell}$ and $d_{nm,\ell}$. Similarly, for the magnetic field, the substitution of (2) in (13) leads to

$$\begin{aligned}
&\frac{1}{\eta_\ell}\sum_{n=1}^{N}\sum_{m=-n}^{n} b_{nm,\ell}\left(\hat{\mathbf{r}}\times\mathbf{m}^{(1)}_{nm,\ell}(R_\ell,\theta,\phi)\right) + a_{nm,\ell}\left(\hat{\mathbf{r}}\times\mathbf{n}^{(1)}_{nm,\ell}(R_\ell,\theta,\phi)\right) + \\
&\frac{1}{\eta_\ell}\sum_{n=1}^{N}\sum_{m=-n}^{n} d_{nm,\ell}\left(\hat{\mathbf{r}}\times\mathbf{m}^{(4)}_{nm,\ell}(R_\ell,\theta,\phi)\right) + c_{nm,\ell}\left(\hat{\mathbf{r}}\times\mathbf{n}^{(4)}_{nm,\ell}(R_\ell,\theta,\phi)\right) = \\
&\frac{1}{\eta_{\ell-1}}\sum_{n=1}^{N}\sum_{m=-n}^{n} b_{nm,\ell-1}\left(\hat{\mathbf{r}}\times\mathbf{m}^{(1)}_{nm,\ell-1}(R_\ell,\theta,\phi)\right) + a_{nm,\ell-1}\left(\hat{\mathbf{r}}\times\mathbf{n}^{(1)}_{nm,\ell-1}(R_\ell,\theta,\phi)\right) + \\
&\frac{1}{\eta_{\ell-1}}\sum_{n=1}^{N}\sum_{m=-n}^{n} d_{nm,\ell-1}\left(\hat{\mathbf{r}}\times\mathbf{m}^{(4)}_{nm,\ell-1}(R_\ell,\theta,\phi)\right) + c_{nm,\ell-1}\left(\hat{\mathbf{r}}\times\mathbf{n}^{(4)}_{nm,\ell-1}(R_\ell,\theta,\phi)\right).
\end{aligned} \tag{15}$$

By inner product of both sides of (14) to $\hat{\mathbf{r}}\times\mathbf{m}^{*(1)}_{nm,\ell-1}(R_\ell,\theta,\phi)$ and integrating over the whole solid angle, using orthogonality relations in Appendix. A, (14) reduces to

$$\begin{aligned}
&h^{(2)}_n(k_{\ell-1}R_\ell)c_{nm,\ell-1} - j_n(k_\ell R_\ell)a_{nm,\ell} \\
&- h^{(2)}_n(k_\ell R_\ell)c_{nm,\ell} = -j_n(k_{\ell-1}R_\ell)a_{nm,\ell-1}.
\end{aligned} \tag{16}$$

Similarly, inner product of both side of (14) to $\hat{\mathbf{r}} \times \mathbf{n}^{*(1)}_{nm,\ell-1}(R_\ell,\theta,\phi)$ leads to

$$\begin{aligned}&\tilde{h}_n^{(2)}(k_{\ell-1}R_\ell)d_{nm,\ell-1} - \tilde{j}_n(k_\ell R_\ell)b_{nm,\ell}\\ &\quad - \tilde{h}_n^{(2)}(k_\ell R_\ell)d_{nm,\ell} = -\tilde{j}_n(k_{\ell-1}R_\ell)b_{nm,\ell-1}\end{aligned} \tag{17}$$

where for the spherical Bessel or Hankel function $z_n^{(i)}(x)$ we define $\tilde{z}_n^{(i)}(x)$ as follow

$$\tilde{z}_n^{(i)}(x) = \frac{1}{x}\frac{d}{dx}\left(xz_n^{(i)}(x)\right) = \frac{n+1}{x}z_n^{(i)}(x) - z_{n+1}^{(i)}(x). \tag{18}$$

In a similar manner to extraction (16) and (17) from (14), the following equations can be extracted from (15)

$$\begin{aligned}&\frac{h_n^{(2)}(k_{\ell-1}R_\ell)}{\eta_{\ell-1}}d_{nm,\ell-1} - \frac{j_n(k_\ell R_\ell)}{\eta_\ell}b_{nm,\ell}\\ &\quad - \frac{h_n^{(2)}(k_\ell R_\ell)}{\eta_\ell}d_{nm,\ell} = -\frac{j_n(k_{\ell-1}R_\ell)}{\eta_{\ell-1}}b_{nm,\ell-1}\end{aligned} \tag{19}$$

$$\begin{aligned}&\frac{\tilde{h}_n^{(2)}(k_{\ell-1}R_\ell)}{\eta_{\ell-1}}c_{nm,\ell-1} - \frac{\tilde{j}_n(k_\ell R_\ell)}{\eta_\ell}a_{nm,\ell}\\ &\quad - \frac{\tilde{h}_n^{(2)}(k_\ell R_\ell)}{\eta_\ell}c_{nm,\ell} = -\frac{\tilde{j}_n(k_{\ell-1}R_\ell)}{\eta_{\ell-1}}a_{nm,\ell-1}.\end{aligned} \tag{20}$$

So, the boundary conditions in the interface of any two adjacent layers result in four independent equations similar to (16), (17), (19) and (20). Thereupon, considering boundary conditions for all interfaces of the multilayer spherical model, the following system of equations may be setup

$$\begin{bmatrix} Z^2_{n,0} & Z^1_{n,1} & 0_{4\times4} & \dots & 0_{4\times2}\\ 0_{4\times2} & Z^2_{n,1} & Z^1_{n,2} & \dots & 0_{4\times2}\\ 0_{4\times2} & 0_{4\times4} & Z^2_{n,2} & \dots & 0_{4\times2}\\ \vdots & \vdots & \vdots & \ddots & \vdots\\ 0_{4\times2} & 0_{4\times4} & 0_{4\times4} & \dots & Z^1_{n,L}\end{bmatrix}\begin{bmatrix} c_{nm,0}\\ d_{nm,0}\\ a_{nm,1}\\ b_{nm,1}\\ c_{nm,1}\\ d_{nm,1}\\ \vdots\\ a_{nm,L}\\ b_{nm,L}\end{bmatrix} = \begin{bmatrix} V_1\\ V_2\\ V_3\\ \vdots\\ V_L\end{bmatrix} \tag{21}$$

with the submatrices of (22)-(25) ((22) and (23) are shown at the button of the page) as the elements of the coefficient matrix

$$Z^2_{\substack{n,0\\1\le n\le N}} = \begin{bmatrix} h_n^{(2)}(k_0R_1) & 0\\ 0 & \tilde{h}_n^{(2)}(k_0R_1)\\ \frac{1}{\eta_0}\tilde{h}_n^{(2)}(k_0R_1) & 0\\ 0 & \frac{1}{\eta_0}h_n^{(2)}(k_0R_1)\end{bmatrix} \tag{24}$$

$$Z^1_{\substack{n,L\\1\le n\le N}} = -\begin{bmatrix} j_n(k_LR_L) & 0\\ 0 & \tilde{j}_n(k_LR_L)\\ \frac{1}{\eta_L}\tilde{j}_n(k_LR_L) & 0\\ 0 & \frac{1}{\eta_L}j_n(k_LR_L)\end{bmatrix}. \tag{25}$$

Furthermore, the elements of the excitation vector on the right-hand side of (21) are

$$V_1 = -\begin{bmatrix} j_n(k_0R_1)a_{nm,0}\\ \tilde{j}_n(k_0R_1)b_{nm,0}\\ \frac{1}{\eta_0}\tilde{j}_n(k_0R_1)a_{nm,0}\\ \frac{1}{\eta_0}j_n(k_0R_1)b_{nm,0}\end{bmatrix}, \quad V_{\substack{\ell\\2\le\ell\le L}} = 0_{4\times1} \tag{26}$$

where the amplitudes of SVWFs of the incident field $a_{nm,0}$ and $b_{nm,0}$ are determined from (10) and (11), respectively. Therefore, (21) may be solved for the unknown amplitudes of SVWFs of the induced fields inside different layers and those of the scattered field outside the external layer.

III. NUMERICAL RESULTS

In this section, some numerical examples are presented to assess the validation of the proposed method. A printed inverted-F antenna (PIFA) is considered the source antenna for all examples. First, the antenna is simulated for the evaluation of the radiated fields, and the amplitudes of their SVWFs are calculated. Then, some spherical head models are exposed to the radiated fields by the PIFA for the evaluation of the induced fields inside the models using the proposed method. The induced fields inside the models as well as the point SAR are compared with the corresponding numerical results of the problem simulation using commercial full-wave software.

A. PIFA RADIATED FIELD SVWFS

Figure 3 shows the geometry and dimensions of the PIFA optimized for operation frequency of $3.5\,GHz$. For the evaluation of the amplitudes of the SWVFs of radiated fields, the antenna is simulated in the full-wave commercial software of

$$Z^1_{\substack{n,\ell\\0<\ell<L\\1\le n\le N}} = -\begin{bmatrix} j_n(k_\ell R_\ell) & 0 & h_n^{(2)}(k_\ell R_\ell) & 0\\ 0 & \tilde{j}_n(k_\ell R_\ell) & 0 & \tilde{h}_n^{(2)}(k_\ell R_\ell)\\ \frac{1}{\eta_\ell}\tilde{j}_n(k_\ell R_\ell) & 0 & \frac{1}{\eta_\ell}\tilde{h}_n^{(2)}(k_\ell R_\ell) & 0\\ 0 & \frac{1}{\eta_\ell}j_n(k_\ell R_\ell) & 0 & \frac{1}{\eta_\ell}h_n^{(2)}(k_\ell R_\ell)\end{bmatrix} \tag{22}$$

$$Z^2_{\substack{n,\ell\\0<\ell<L\\1\le n\le N}} = \begin{bmatrix} j_n(k_\ell R_{\ell+1}) & 0 & h_n^{(2)}(k_\ell R_{\ell+1}) & 0\\ 0 & \tilde{j}_n(k_\ell R_{\ell+1}) & 0 & \tilde{h}_n^{(2)}(k_\ell R_{\ell+1})\\ \frac{1}{\eta_\ell}\tilde{j}_n(k_\ell R_{\ell+1}) & 0 & \frac{1}{\eta_\ell}\tilde{h}_n^{(2)}(k_\ell R_{\ell+1}) & 0\\ 0 & \frac{1}{\eta_\ell}j_n(k_\ell R_{\ell+1}) & 0 & \frac{1}{\eta_\ell}h_n^{(2)}(k_\ell R_{\ell+1})\end{bmatrix} \tag{23}$$

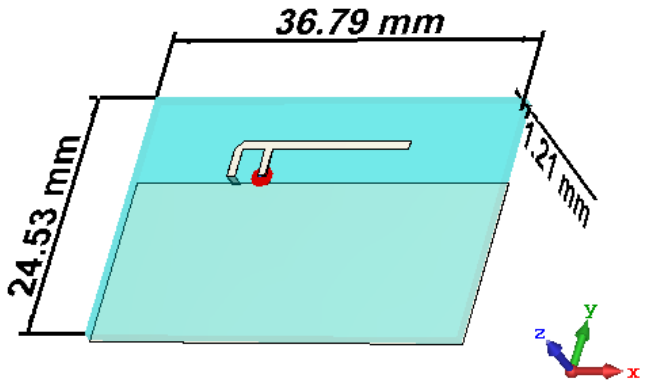

FIGURE 3. Geometry and dimensions of a PIFA optimized for operation at $f = 3.5$ GHz.

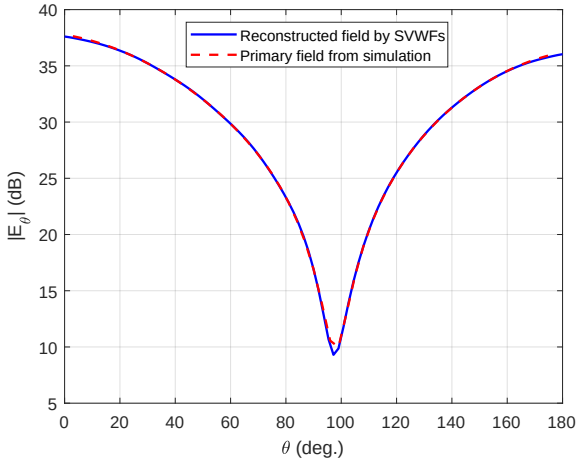

FIGURE 4. Comparison of E_θ components of reconstructed and primary electric field radiated by the PIFA shown in Figure 3 at $\phi = 0^\circ$.

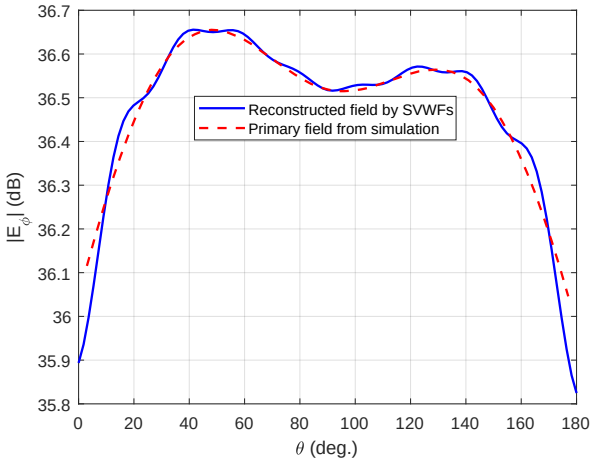

FIGURE 5. Comparison of E_ϕ components of reconstructed and primary electric field radiated by the PIFA shown in Figure 3 at $\phi = 0^\circ$.

CST Studio Suite [19]. Electric and magnetic fields radiated by the antenna are sampled on a sphere of radius $7\,cm$

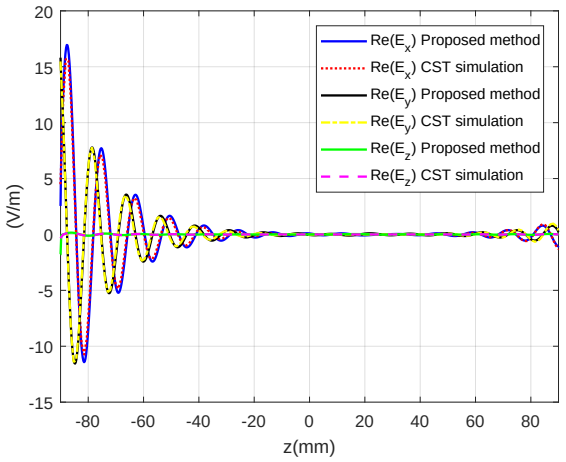

FIGURE 6. Comparison of the real part of different components of the electric field inside the homogeneous spherical head model evaluated from the proposed method with those of simulation by CST.

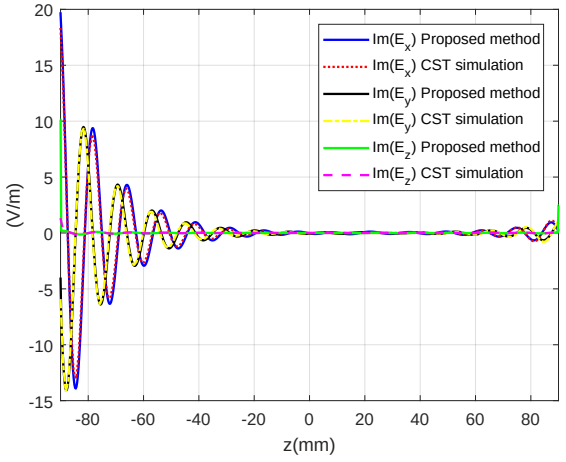

FIGURE 7. Comparison of the imaginary part of different components of the electric field inside the homogeneous spherical head model evaluated from the proposed method with those of simulation by CST.

encompassing it. The amplitudes of the SWVFs of radiated fields are calculated using (5) and (6) in the coordinate system with the origin at the center of the sampling sphere. For the verification of this process, the electric field radiated by the antenna is reconstructed through the substitution of computed amplitudes of the SVWFs in (1) and (2), where superscript $i = 4$ associated with the Hankel function of the second kind is used for the satisfaction of the radiation conditions at far distances from the origin. Figure 4 shows the E_θ component of the reconstructed electric field in comparison with that of the primary field from simulation for $\theta = [0^\circ, 180^\circ]$ at $\phi = 0^\circ$ on the surface of sampling sphere. A similar comparison is made in Figure 5 for E_ϕ component of the radiated electric field. The acceptable consistency between the reconstructed and the primary radiated fields verifies the process for the evaluation of amplitudes of the

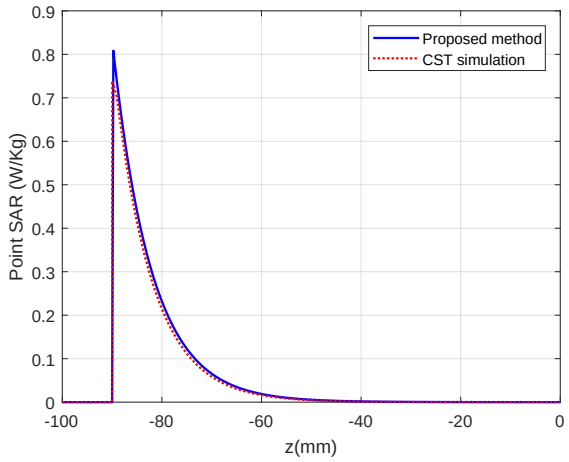

FIGURE 8. Comparison of point SAR inside the homogeneous spherical head model evaluated from the proposed method with that of simulation by CST.

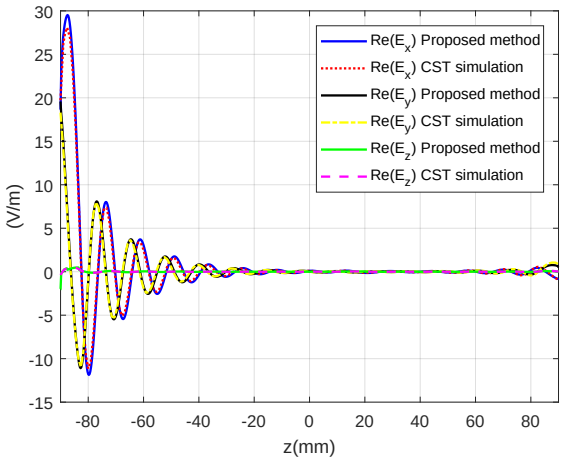

FIGURE 9. Comparison of the real part of different components of the electric field inside the multilayer spherical head model evaluated from the proposed method with those of simulation by CST.

TABLE 1. Parameters of multilayer spherical head model according to tissue properties from [20]

ℓ	Tissue	ε_{r_ℓ}	σ_ℓ (S/m)	R_ℓ (mm)	ρ_ℓ (Kg/m^3)
1	Skin	37.0	2.02	90.0	1109
2	Fat	10.5	0.42	89.0	911
3	Bone (Cancellous)	17.4	1.20	87.6	1178
4	Dura	40.7	2.37	83.5	1174
5	CSF	64.6	4.57	83.0	1007
6	Brain (Gray matter)	47.3	2.64	81.0	1045

SVWFs of radiated fields. The verification has also been tested through similar comparisons of the radiated fields on the surface of the spheres of radii greater than the radius of the sampling sphere with satisfactory results, that are not reported here due to the space limitation.

B. HOMOGENEOUS SPHERICAL HEAD MODEL EXPOSED TO RADIATION OF PIFA

In this section, a homogeneous sphere of radius $R_1 = 9\,cm$ is considered as a simple model of the human head. Such a model has been considered in many similar works for the assessment of the correctness of their proposed method. Here, the dielectric properties of the model are considered like those of the gray matter tissue of the human brain with the relative permittivity of $\varepsilon_{r_1} = 47.3$ and conductivity of $\sigma_1 = 2.64\,S/m$ at the examination frequency of $3.5\,GHz$ [20]. The aforementioned PIFA is located at $z = -16\,cm$ in the coordinate system with the origin at the center of the spherical model (refer to Figure 1). Figure 6 shows the real part of different components of the electric field along $z-$axis, evaluated from the proposed method inside the homogeneous head model in comparison with those of the numerical time-domain simulation of the problem in CST Studio Suite. Similar comparisons are also shown in Figure 7 for the imaginary parts of the different components of the electric field. Assuming the mass density of $\rho_1 = 1045\,Kg/m^3$ for the gray matter tissue [20], the point specific absorption rate (SAR) is also evaluated as follow

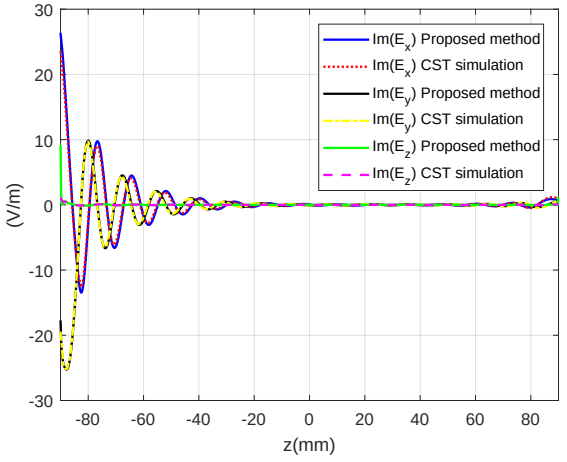

FIGURE 10. Comparison of the imaginary part of different components of the electric field inside the multilayer spherical head model evaluated from the proposed method with those of simulation by CST.

$$SAR(\mathbf{r}) = \frac{\sigma(\mathbf{r})}{2\rho(\mathbf{r})}|\mathbf{E}^{inc}(\mathbf{r}) + \mathbf{E}^{sca}(\mathbf{r})|^2. \qquad (27)$$

A comparison between the evaluated point SAR using the proposed method and that of the numerical simulation in CST Studio Suite is shown in Figure 8. The consistency between the results of the proposed method and those of the numerical simulation can verify the proposed method, here for a homogeneous spherical head model.

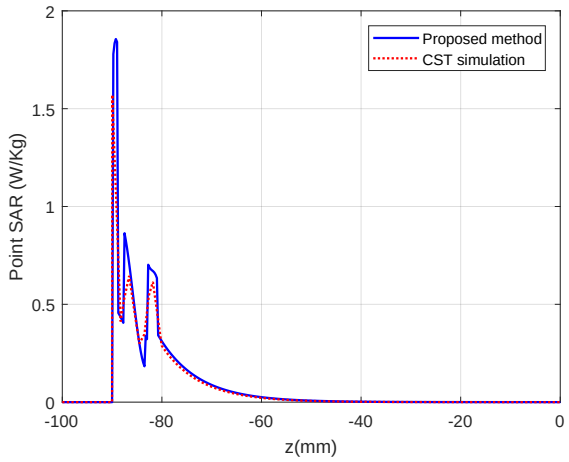

FIGURE 11. Comparison of point SAR inside the multilayer spherical head model evaluated from the proposed method with that of simulation by CST.

C. SIX-LAYER SPHERICAL HEAD MODEL EXPOSED TO RADIATION OF PIFA

In this section, a six-layer spherical head model is considered. Mass densities, conductivity, and relative permittivity of each layer at the examination frequency of $3.5\,GHz$ [20] as well as their supposed radii are reported in Table 1.

Comparisons similar to the previous example for the real and imaginary parts of different components of the electric field inside the head model are shown in Figure 9 and Figure 10, respectively. For this example, the comparison between the point SAR evaluated from the proposed method and that of CST simulation is shown in Figure 11. The consistency between the results of the proposed method and those of the numerical simulation verifies the proposed method, here for a multilayer spherical head model.

IV. CONCLUSIONS

In this paper, a semi-analytical method has been presented for the evaluation of the electromagnetic fields induced inside a multilayer spherical head model irradiated by an arbitrary source antenna. The source antenna has been simulated numerically by a commercial full-wave software. The radiated electromagnetic fields by the antenna have been sampled on a spherical surface encompassing the antenna structure. The amplitudes of SVWFs corresponding to the antenna radiated fields have been evaluated and using the translation addition theorem, they have been translated to the coordinate system originating from the center of the spherical head model. Finally, by considering the boundary conditions on the interfaces of different layers of the multilayer spherical head model, a system of equations has been set up for the unknown amplitudes of SVWFs inside the spherical model. The reaction of the spherical head model to the source antenna was neglected since the head model was supposed to be at a sufficient distance from the antenna. The verification of the proposed method has been shown through the comparison of its results with those of the full-wave simulation of the overall problem in a commercial software. In comparison with a full-wave solver, the proposed method facilitates the problem solution where it should be repeated by new models or various distances between the antenna and head model. In another word, the proposed method makes it possible to repeat the solution for new models made from different material properties or the number of layers or thicknesses, or even for different distances between the antenna and head model, without the need to repeat the analysis of the antenna structure.

APPENDIX.

A. ORTHOGONALITY RELATIONS FOR TRANSVERSE COMPONENTS OF SVWFS

The following orthogonality relations for the transverse components of SVWFs may be extracted from their general orthogonality relation [9]

$$\left\langle \left(\hat{\mathbf{r}} \times \mathbf{m}^{*(i)}_{nm,\ell}(r,\theta,\phi)\right) . \left(\hat{\mathbf{r}} \times \mathbf{m}^{(i')}_{n'm',\ell'}(r,\theta,\phi)\right) \right\rangle = 4\pi \frac{n(n+1)}{2n+1} \frac{(n+m)!}{(n-m)!} z^{*(i)}_n(k_\ell r) z^{(i')}_n(k_{\ell'} r) \delta_{n,n'} \delta_{m,m'} \tag{A.1}$$

$$\left\langle \left(\hat{\mathbf{r}} \times \mathbf{n}^{*(i)}_{nm,\ell}(r,\theta,\phi)\right) . \left(\hat{\mathbf{r}} \times \mathbf{n}^{(i')}_{n'm',\ell'}(r,\theta,\phi)\right) \right\rangle = 4\pi \frac{n(n+1)}{2n+1} \frac{(n+m)!}{(n-m)!} \tilde{z}^{*(i)}_n(k_\ell r) \tilde{z}^{(i')}_n(k_{\ell'} r) \delta_{n,n'} \delta_{m,m'} \tag{A.2}$$

$$\left\langle \left(\hat{\mathbf{r}} \times \mathbf{m}^{*(i)}_{nm,\ell}(r,\theta,\phi)\right) . \left(\hat{\mathbf{r}} \times \mathbf{n}^{(i')}_{n'm',\ell'}(r,\theta,\phi)\right) \right\rangle = 0 \tag{A.3}$$

where $\delta_{p,q}$ is Kronecker delta function, $\tilde{z}^{(i)}_n(x)$ is defined in (18) and for the vector functions $\mathbf{X}(r,\theta,\phi)$ and $\mathbf{Y}(r,\theta,\phi)$

$$\langle \mathbf{X}(r,\theta,\phi).\mathbf{Y}(r,\theta,\phi) \rangle = \oint_{4\pi} \mathbf{X}(r,\theta,\phi).\mathbf{Y}(r,\theta,\phi) d\Omega \tag{A.4}$$

where Ω denotes the solid angle with the apex at the origin of the coordinate system.

B. COEFFICIENTS OF SVWFS TRANSLATION ADDITION THEOREM

The coefficients of the translation addition theorem in section II-C are defined as follows [18]

$$\begin{aligned}C(\mu,\nu|m,n) &= \alpha(\mu,\nu|m,n)\\ &+\frac{k_0R_0\cos\theta_0}{2n+3}\frac{n+m+1}{n+1}\alpha(\mu,\nu|m,n+1)\\ &+\frac{k_0R_0\cos\theta_0}{2n-1}\frac{n-m}{n}\alpha(\mu,\nu|m,n-1)\\ &+\frac{k_0R_0\sin\theta_0\exp(-j\phi_0)}{2(2n+3)(n+1)}\alpha(\mu,\nu|m-1,n+1)\\ &-\frac{k_0R_0\sin\theta_0\exp(-j\phi_0)}{2(2n-1)n}\alpha(\mu,\nu|m-1,n-1)\\ &-\frac{k_0R_0\sin\theta_0\exp(j\phi_0)}{2(2n+3)}\frac{(n+m+2)(n+m+1)}{n+1}\\ &\times\alpha(\mu,\nu|m+1,n+1)\\ &+\frac{k_0R_0\sin\theta_0\exp(j\phi_0)}{2(2n-1)}\frac{(n-m-1)(n-m)}{n}\\ &\times\alpha(\mu,\nu|m+1,n-1)\end{aligned} \tag{B.1}$$

$$\begin{aligned}D(\mu,\nu|m,n) &= \frac{jk_0R_0\cos\theta_0}{n(n+1)}m\alpha(\mu,\nu|m,n)\\ &+\frac{jk_0R_0\sin\theta_0\exp(-j\phi_0)}{2n(n+1)}\alpha(\mu,\nu|m-1,n)\\ &+\frac{jk_0R_0\sin\theta_0\exp(j\phi_0)}{2n(n+1)}(n+m+1)(n-m)\\ &\times\alpha(\mu,\nu|m+1,n)\end{aligned} \tag{B.2}$$

where $R_0 = R_1 + d$, (R_0, θ_0, ϕ_0) are the coordinates of the position vector of the origin of (x, y, z) coordinate system in (x', y', z') coordinate system, and

$$\begin{aligned}\alpha(\mu,\nu|m,n) &= \sum_p j^{n+p-\nu}(2n+1)\frac{(n-m)!}{(n+m)!}\\ &\times a(\mu,\nu|m,n|p)h_p^{(2)}(k_0R_0)P_p^{\mu-m}(\cos\theta_0)e^{j(\mu-m)\phi_0}\end{aligned} \tag{B.3}$$

in which

$$\begin{aligned}a(\mu,\nu|m,n|p) &= (-1)^\mu(2p+1)\\ &\times\sqrt{\frac{(\nu+\mu)!(n+m)!(p-\mu+m)!}{(\nu-\mu)!(n-m)!(p+\mu-m)!}}\\ &\times\begin{pmatrix}\nu & n & p\\ 0 & 0 & 0\end{pmatrix}\begin{pmatrix}\nu & n & p\\ \mu & -m & -\mu+m\end{pmatrix}\end{aligned} \tag{B.4}$$

and the factor $\begin{pmatrix}j_1 & j_2 & j_3\\ m_1 & m_2 & m_3\end{pmatrix}$ is Wigner 3-j symbol which has been associated with the coupling of angular momentum in quantum mechanics [21], [22].

REFERENCES

[1] K. S. Nikita, M. Cavagnaro, P. Bernardi, N. K. Uzunoglu, S. Pisa, E. Piuzzi, J. N. Sahalos, G. I. Krikelas, J. A. Vaul, P. S. Excell et al., "A study of uncertainties in modeling antenna performance and power absorption in the head of a cellular phone user," IEEE Transactions on Microwave Theory and Techniques, vol. 48, no. 12, pp. 2676–2685, 2000.

[2] H. Khodabakhshi and A. Cheldavi, "Irradiation of a six-layered spherical model of human head in the near field of a half-wave dipole antenna," IEEE transactions on microwave theory and techniques, vol. 58, no. 3, pp. 680–690, 2010.

[3] X. Kang, L. Li, M. Leong, and P. Kooi, "A method of moments study of SAR inside spheroidal human head and current distribution along handset wire antennas," Journal of Electromagnetic Waves and Applications, vol. 15, no. 1, pp. 61–75, 2001.

[4] S. K. Khamas, "Electromagnetic radiation by antennas of arbitrary shape in a layered spherical media," IEEE transactions on antennas and propagation, vol. 57, no. 12, pp. 3827–3834, 2009.

[5] L. Li, W. Yu, and R. Mittra, "Computation of SAR levels in SAM's head model located inside an automobile via the parallel FDTD algorithm," in 2010 International Conference on Applications of Electromagnetism and Student Innovation Competition Awards (AEM2C). IEEE, 2010, pp. 24–28.

[6] K. Masumnia-Bisheh, M. Ghaffari-Miab, and B. Zakeri, "Evaluation of different approximations for correlation coefficients in stochastic FDTD to estimate SAR variance in a human head model," IEEE Transactions on Electromagnetic Compatibility, vol. 59, no. 2, pp. 509–517, 2016.

[7] F. Ç. Kunter, C. Gunduz, and S. S. Seker, "Computation of SAR and temperature values in the human head due to 2G, 3G, 4G mobile wireless systems," Journal of Aeronautics and Space Technologies, vol. 11, no. 1, pp. 1–6, 2018.

[8] L. Belrhiti, F. Riouch, A. Tribak, J. Terhzaz, and A. M. Sanchez, "Investigation of dosimetry in four human head models for planar monopole antenna with a coupling feed for LTE/WWAN/WLAN internal mobile phone," Journal of Microwaves, Optoelectronics and Electromagnetic Applications, vol. 16, pp. 494–513, 2017.

[9] J. E. Hansen, Spherical near-field antenna measurements. IET, 1988, vol. 26.

[10] J. A. Stratton, Electromagnetic theory. John Wiley & Sons, 2007, vol. 33.

[11] C. Liang and Y. Lo, "Scattering by two spheres," Radio Science, vol. 2, no. 12, pp. 1481–1495, 1967.

[12] M. Alian and H. Oraizi, "Electromagnetic multiple PEC object scattering using equivalence principle and addition theorem for spherical wave harmonics," IEEE Transactions on Antennas and Propagation, vol. 66, no. 11, pp. 6233–6243, 2018.

[13] M. Alian and H. Oraizi, "Application of equivalence principle for EM scattering from irregular array of arbitrarily oriented PEC scatterers using both translation and rotation addition theorems," IEEE Transactions on Antennas and Propagation, vol. 67, no. 5, pp. 3256–3267, 2019.

[14] W. C. Chew, E. Michielssen, J. Song, and J.-M. Jin, Fast and efficient algorithms in computational electromagnetics. Artech House, Inc., 2001.

[15] R. H. MacPhie and K.-L. Wu, "A plane wave expansion of spherical wave functions for modal analysis of guided wave structures and scatterers," IEEE Transactions on Antennas and Propagation, vol. 51, no. 10, pp. 2801–2805, 2003.

[16] F. Jensen and A. Frandsen, "On the number of modes in spherical wave expansions," Proc. 26th AMTA, vol. 2, no. 1, pp. 489–494, 2004.

[17] B. Friedman and J. Russek, "Addition theorems for spherical waves," Quarterly of Applied Mathematics, vol. 12, no. 1, pp. 13–23, 1954.

[18] S. Stein, "Addition theorems for spherical wave functions," Quarterly of Applied Mathematics, vol. 19, no. 1, pp. 15–24, 1961.

[19] "CST studio suite 2019," Darmstadt, Germany, 2019.

[20] P. Hasgall, F. Di Gennaro, C. Baumgartner, E. Neufeld, B. Lloyd, M. Gosselin, D. Payne, A. Klingenböck, and N. Kuster, "IT'IS Database for thermal and electromagnetic parameters of biological tissues," https://itis.swiss/virtual-population/tissue-properties/database/, 2018.

[21] E. P. Wigner and U. Fano, "Group theory and its application to the quantum mechanics of atomic spectra," American Journal of Physics, vol. 28, no. 4, pp. 408–409, 1960.

[22] A. R. Edmonds, Angular momentum in quantum mechanics. Princeton university press, 2016.